

ORIGINAL ARTICLE

Deficits in the IgG⁺ memory B-cell recovery after anthracycline treatment is confined to the spleen of rhesus macaques

Gintare Lasaviciute¹, Andréas L Bricaud², Fredrika Hellgren^{3,4}, Hanna M Ingelman-Sundberg², Staffan Eksborg², Margreet Jonker⁵, Krista G Haanstra⁵, Ida Hed Myrberg², Eva Sverremark-Ekström¹, Karin Loré^{3,4}, Shanie Saghafian-Hedengren^{1,2†}  & Anna Nilsson^{2†}

¹Department of Molecular Biosciences, The Wenner-Gren Institute, Stockholm University, Stockholm, Sweden

²Childhood Cancer Research Unit, Department of Women's and Children's Health, Karolinska Institutet, Stockholm, Sweden

³Department of Medicine Solna, Division of Immunology and Allergy, Karolinska Institutet and Karolinska University Hospital, Stockholm, Sweden

⁴Center for Molecular Medicine, Karolinska Institutet, Stockholm, Sweden

⁵Biomedical Primate Research Centre (BPRC), Rijswijk, The Netherlands

Correspondence

S S-Hedengren, Childhood Cancer Research Unit, Department of Women's and Children's Health, Karolinska Institutet, Tomtebodavägen 18A, Floor 8, 171 77 Stockholm, Sweden.
E-mail: shanie.hedengren@ki.se

[‡]SSH and AN shared last authorship

[†]Equal contributors.

Received 14 November 2019;

Revised 8 June 2020;

Accepted 8 June 2020

doi: 10.1002/cti.1150

Clinical & Translational Immunology
2020; 9: e1150

Abstract

Objectives. Loss of vaccine-induced antibodies (Abs) after chemotherapy against paediatric acute lymphoblastic leukaemia (ALL) is common and often necessitates re-immunisation after cessation of treatment. Even so, some ALL survivors fail to mount or to maintain protective Abs. Germinal centres (GCs) are clusters of proliferating B cells in follicles of secondary lymphoid tissues (SLTs) formed during adaptive immune responses and the origins of long-lived memory B and plasma cells that are the source of Abs. Furthermore, productive GC reactions depend on T follicular helper (T_{FH}) cells. To understand why chemotherapy induces deficits in Ab responses, we examined how SLTs were affected by chemotherapy. **Methods.** Rhesus macaques were infused with either three cycles of the anthracycline doxorubicin or saline, followed by immunisation with a *de novo* and booster antigen. Spleen and lymph nodes were removed, and memory B, bulk T and T_{FH} cells were examined. **Results.** Despite adequate GC morphology, a diminished memory and IgG⁺ B-cell population along with diminished total and booster vaccine-specific IgG-producing memory B cells were noted in the spleens of macaques with past doxorubicin exposure compared to the saline-treated controls ($P < 0.05$). Intact bulk T and T_{FH} cells were found in the SLTs of treated macaques, which displayed higher CD40L upregulation capacity by their splenic CXCR5⁺ helper T cells ($P < 0.01$). In contrast to the spleen, the immune cell populations studied were comparable between the lymph nodes of both saline- and doxorubicin-treated macaques. **Conclusion.** Our findings suggest that the splenic memory B-cell subset, compared to its lymph node counterpart, is more severely altered by anthracycline treatment.

Keywords: anthracycline, *de novo* and booster vaccine, memory B-cell response, rhesus macaque, secondary lymphoid organs

INTRODUCTION

Many patients lose their previous vaccine-induced antibody (Ab) titres following completion of chemotherapy against paediatric acute lymphoblastic leukaemia (ALL). In the clinical context, this often requires re-administration of childhood vaccines after cancer treatment. Even so, a subset of these patients fails to regain adequate humoral immunity, evidenced by lasting insufficiencies in the establishment or maintenance of protective Ab levels following repeated immunisations.¹

Vaccine-specific Ab titres are maintained by terminally differentiated, long-lived plasma cells (LLPCs) in the bone marrow, which originate from B cells undergoing the late stages of germinal centre (GC) reactions in secondary lymphoid tissues (SLTs).² If the first line of defence mediated by circulating Abs is breached, the existing pool of pathogen-specific memory B cells (MBCs) will undergo clonal expansion and ultimately replenish the LLPC pool. In both human and rhesus macaques (from now on referred to as macaques), the MBC population is currently identified by CD27 expression, a costimulatory molecule that is considered a surrogate for the presence of somatic hypermutation. Nonetheless, a sizeable proportion of IgG⁺ *bona fide* MBCs in the blood and SLTs lack surface CD27 expression.^{3,4} Activation of MBCs leads to downregulation of CD21, which further distinguishes classical (also called resting) CD27⁺CD21⁺ from activated CD27⁺CD21⁻ MBCs.⁵ It has been suggested that B cells lacking both CD27 and CD21 correspond to atypical or exhausted MBCs, which are enriched during chronic immune activation.^{6,7}

Memory T cells consist of two main subsets with distinct phenotypes, migratory capacities and functions. Central memory T cells (T_{CM}), enriched within CD28⁺CD95⁺ T cells, mainly recirculate to the lymph nodes (LNs) and lack immediate effector functions. Effector memory T cells (T_{EM}), enriched within CD28⁻CD95⁺ T cells, primarily home towards peripheral sites and possess immediate effector functions following antigen recognition.⁸ A T-cell type critical for the formation of GCs, and subsequent B-cell

proliferation and maturation in SLTs, is the T follicular helper (T_{FH}) cell, which mediates many of its effects on B cells through IL-21. The canonical marker CXCR5 and high PD-1 expression on CD4⁺ (helper) T cells have been used to identify T_{FH} cells in both humans and macaques. Furthermore, a high T-cell PD-1 expression, colocalised with GC markers, identifies T_{FH} cells found in the SLTs of macaques.⁹

To address how chemotherapy against ALL influences the cells and organs implicated in immunological memory to vaccines, we focused on the anthracycline doxorubicin (Doxo), which is a widely used component in childhood ALL treatment protocols.¹⁰ Furthermore, to avoid the possible impact of leukaemia itself on our read-outs, we utilised nonleukaemic healthy macaques as our study model and treated them with consecutive dosages of the chosen anthracycline. Previously, we had observed unaltered vaccine-specific Ab titres in these animals and a robust reconstitution of their circulating MBC pool one month after cessation of chemotherapy.¹¹ The majority of lymphocytes are, however, found in SLTs,¹² and the nonacute effect of Doxo on cells implicated in immunological memory in these organs remained to be examined. In this follow-up study, we addressed the influence of Doxo on the spleen and LN lymphocytes in the same cohort nearly six months after completion of Doxo treatment and found a diminished total IgG and booster vaccine-specific IgG response by splenic MBCs in macaques with past exposure to chemotherapy. To our knowledge, we are the first to study the effect of chemotherapy on SLTs in a large animal model, and we show data suggesting that anthracycline treatment has a long-lasting imprint on the splenic MBC population.

RESULTS

The spleens of macaques with past Doxo treatment contain lower proportions of MBCs and IgG⁺ B cells despite the ability to form detectable GCs

To get an insight into the characteristics of B lymphocytes from SLTs of Doxo-treated animals at the single-cell level, we immunophenotyped the

B-cell compartment in the spleen and LN from each animal (Figure 1a and b, representative gating strategies). We found significantly lower proportions of splenic MBC and surface IgG⁺ B cells ($P < 0.05$ for both, Figure 1c) in the group of Doxo-treated macaques than in the saline group, whereas the proportions of LN MBCs, on the other hand, seemed intact (Figure 1d). Overall, the spleens from all macaques contained a sizeable population of CD27^{hi}CD38^{hi} cells (Figure 1a and b), accounting for > 1.0% of live B cells in 9 of 10 animals. This plasmablast phenotype was less frequent in the LN, accounting for > 1.0% of live B cells in 3 of 10 animals (Figure 1e and f). Furthermore, we noticed a difference in the distribution of activated and resting MBC phenotypes according to the type of SLT; an activated MBC phenotype dominated in the spleens, while the majority of MBCs in the LNs of all animals were resting MBCs (Figure 1a, b, e, f). There was a significantly higher proportion of activated MBCs within the spleen compared to LNs [median 16.1% (min–max 6.9–44.6%) and median 7.1% (min–max 1.5–12.4%), respectively, $P < 0.01$] in the saline-treated animals. No statistical difference was found following comparison of the activated MBCs in the spleen and LNs of Doxo-exposed macaques [median 10.4% (min–max 4.7–21.5%) and median 2.7% (min–max 0.5–14.9%), respectively, $P = 0.63$]. Corresponding statistical evaluation of resting MBCs across SLTs in each treatment group revealed no significant differences (data not shown).

Neither SLT contained any detectable CD138⁺ cells derived from the plasmablast gate (blue gated population, Figure 1a and b) or CD38^{hi} B cells which correspond to PC precursors (Figure 1a and b). Examination of splenic GC morphology revealed an intact ability to form GCs in the Doxo-treated group (Supplementary figure 1), and the proportion of splenic CD21^{hi} B cells was comparable between the Doxo- and saline-treated groups [median 7.8% (min–max: 4.5–12.6%) and median 7.4% (min–max: 3.8–20.3), respectively]. No significant differences were found in splenic or LN CD10⁺ B-cell or atypical MBC frequencies between the two groups (data not shown). Cluster and principal component analyses were applied to evaluate whether it was possible to group the animals into Doxo-treated and nontreated on the basis of their B-cell flow cytometric profiles by considering all splenic B-cell

subsets or MBCs at the same time, but no distinct clustering of the two treatment groups emerged (data not shown).

Diminished numbers of IgG-producing MBCs in the spleens of macaques with past Doxo exposure

We next examined whether there was a connection between B-cell Ab production and the altered proportions of IgG⁺ B cells and MBCs observed in the SLTs of Doxo-treated animals. Nearly all animals had a noticeable number of spontaneous IgG-producing cells (ASCs) in their spleens regardless of Doxo treatment or not (Figure 2a, Ctrl). Following activation of MBCs, we noticed significantly fewer IgG-secreting cells in animals with past Doxo treatment ($P < 0.05$, Figure 2a, I + R). With regard to antibody production in LNs, we observed a comparable pattern and quantity of IgG-secreting cells in both groups following MBC activation, whereas spontaneous IgG-producing cells were not as apparent as in the spleen (Figure 2b). In addition to bulk IgG secretion by MBCs, their responding capacity to antigens was assessed by examining a *de novo* response (TT antigen, Figure 2c and d) as well as a recall response (measles antigen, Figure 2e and f). The response to TT, in terms of IgG-secreting MBC numbers, was similar between animals with past Doxo treatment and those treated with saline, both in the spleen and in LNs (I + R, Figure 2c and d). However, as Doxo-treated animals had diminished numbers of IgG-producing MBCs in their spleens (I + R, Figure 2a), the proportion of TT-responding MBCs in the Doxo-treated group exceeded that of the saline group ($P < 0.05$, Figure 2c). Neither group of animals had any observable numbers of TT-specific ASCs in their spleen or LNs (Ctrl, Figure 2c and d). In contrast to the B-cell response to the *de novo* TT antigen, which was comparable between the two groups, macaques with past chemotherapy had lower numbers of splenic measles-specific IgG-secreting MBCs ($P < 0.05$, I + R, Figure 2e), which was not observed in the LNs (I + R, Figure 2f). The ratio of measles-specific IgG-producing cells did not differ between the Doxo- and saline-treated groups (Figure 2e and f). Interestingly, regardless of treatment, all animals had observable numbers of measles-specific ASCs, both in their spleens and in LNs (Ctrl, Figure 2e and f). There were no significant differences in

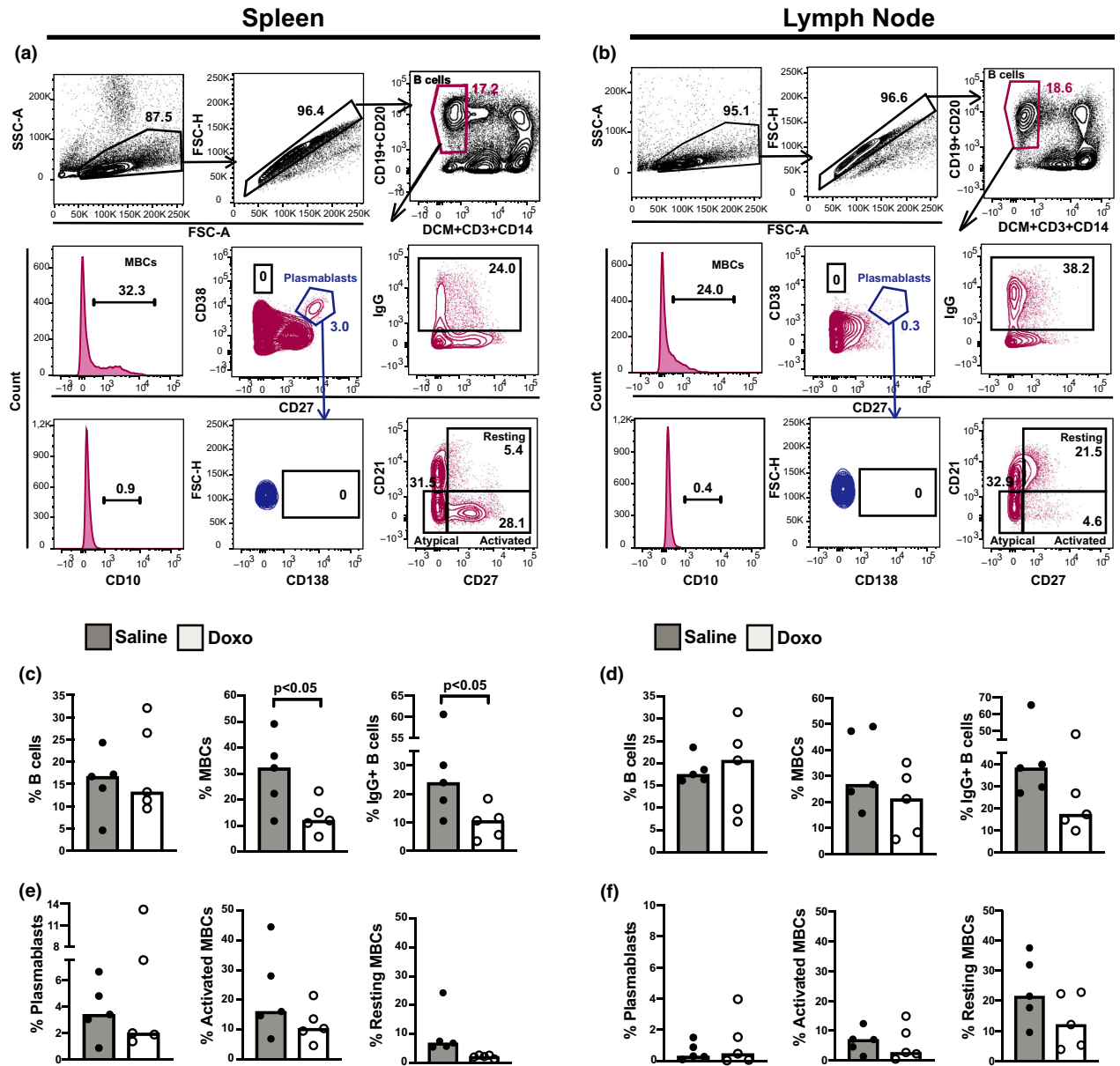


Figure 1. Immunophenotype analysis of spleen and LN MCs from Doxo- and saline-treated macaques. Representative gating strategy for (a) spleen and (b) LN from rhesus macaques ($n = 10$) 5 months postchemotherapy. Compiled data from Doxo (open circles, $n = 5$)- and saline (filled circles, $n = 5$)-treated macaque B cells (DCM⁻CD3⁻CD14⁻CD19⁺CD20⁺), MBCs (CD27⁺ B cells), IgG + B cells and plasmablasts (CD27^{hi}CD38^{hi} B cells) from spleen (c) and LN (d). Proportions of activated memory (CD21⁻CD27⁺) and resting memory (CD21⁺CD27⁺) B cells from the spleen (e) and LN (f). Data are based on 2 replicates. DCM, dead cell marker.

the serum levels of BAFF [mean 378 pg mL⁻¹ (min-max: 223–526) and mean 296 pg mL⁻¹ (min-max: 207–361), respectively] or serum levels of CXCL12 [mean 541 pg mL⁻¹ (min-max: 353–765) and mean 647 pg mL⁻¹ (min-max: 310–1142), respectively] between the Doxo- and saline-treated groups.

The levels of total IgG and IgA were measured in MC culture supernatants of SLTs to assess the connection between bulk Ab-producing cell activity and the ELISPOT findings obtained. Despite a general pattern of higher IgG production in MC cultures from saline-treated animals, the total IgG levels did not significantly

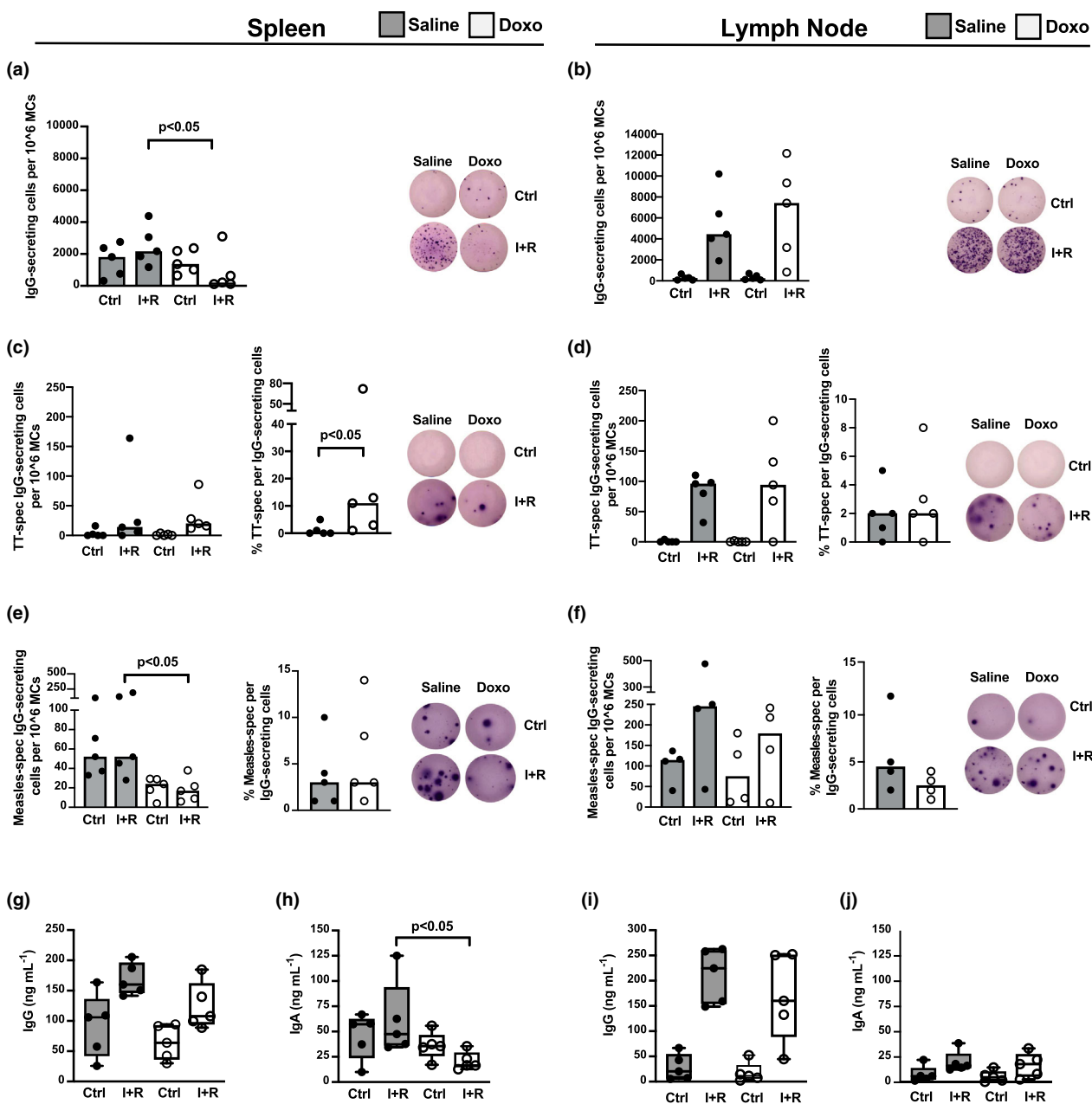


Figure 2. Quantitation of MBCs in SLTs of macaques previously treated with anthracycline. Total IgG (a, b), *de novo* antigen TT (c, d) and booster antigen measles (e, f)-specific IgG response in SLTs of rhesus macaques ($n = 10$) 5 months after completion of chemotherapy. Representative captures from ELISPOT wells with total IgG-spot formation from spleen (right-hand side in a) and LN (right-hand side in b) cells. TT-specific IgG-spot formation from spleen (right-hand side in c) and LN (right-hand side in d) cells, and measles-specific IgG-spot formation from spleen (right-hand side in e) and LN (right-hand side in f) cells. Compiled data in diagrams (left-hand side in a–f). Each condition was set up in 2–4 technical replicates. Total IgG and IgA levels in MC culture supernatants from spleen (g, h) and LN (i, j) quantified by ELISA (2 technical replicates per condition). Ctrl, cell culture medium; I + R, IL-2 + R848. Open circles: Doxo-treated. Filled circles: saline-treated macaques ($n = 5$ per group in all experiments except $n = 4$ per group for f).

differ between Doxo- and saline-treated groups (Figure 2g and i). Total IgA levels were significantly lower in the splenic- ($P < 0.05$) but

not the LN-derived MC cultures from Doxo-treated compared to saline-treated macaques (Figure 2h and j, respectively).

Influence of Doxo on T_{FH} cell phenotype, costimulatory capacity and IL-21 production

We next focused on CXCR5⁺ helper T (Th) and T_{FH} cells in SLTs and compared their phenotypes and IL-21 production capacity (Figure 3). In all animals, we noticed a pattern of the LNs containing a larger CXCR5⁺ Th cell population than the spleen, while T_{FH} and CD40L⁺ CXCR5⁺ Th cells were generally less enriched in the LNs (Figure 3a–d). However, no marked differences were found between the Doxo- and saline-treated groups in terms of CXCR5⁺ Th cells or their subset proportions (Figure 3a–d), nor in their IL-21 production ability (Figure 3e and f). The capacity of each CXCR5⁺ Th cell to upregulate CD40L (GeoMFI) following activation was markedly higher in the spleens of Doxo-treated macaques (Figure 3e). This difference was lost upon stratification of the CXCR5⁺ Th cells into T_{FH} cell phenotype (data not shown).

In addition, the functional capacity of T_{FH} cells in SLTs was addressed through IL-21 ELISPOT and ELISA. Collectively, the results showed similar numbers of IL-21-secreting MCs and similar soluble IL-21 levels, from the spleen and LNs of Doxo- and saline-treated macaques (Figure 3g and h). No substantial differences were found between the treatment groups following flow cytometric analysis, in the classical, CD4⁺ and CD8⁺, T-cell compartment (Figure 4a–h, Supplementary table 1), or their intracellular IFN- γ after polyclonal activation (Figure 4c, d, g, h), or their capacity to release IL-4 or TGF- β (Supplementary figure 2).

DISCUSSION

Advances in the treatment and management of ALL have resulted in increasing overall survival rates over the past decades. However, these advances come at other health costs, including diminished protective Abs and loss of LLPCs in paediatric ALL patients.¹³ Currently, the relationship between treatment duration or intensity, or the haematological malignancy itself, and the failure to establish immunological memory after chemotherapy is unclear.¹ Likewise, the tissue distribution of chemotherapeutic agents against ALL and their impact on SLTs of humans is not well-studied. We considered macaques as adequate models to study how anthracycline, one of the most common components included in treatment protocols against ALL, impacts adaptive immune cells,^{14,15} with the advantage of excluding blood

malignancy as a confounding variable of Doxo pharmacodynamics.^{16–18} Furthermore, consecutive sampling from each animal, including sampling of the bone marrow, was feasible.¹¹ Although real-time *in vivo* imaging has been evaluated as a noninvasive method for tracing lymphocyte recovery in SLTs postimmunosuppression in macaques,¹⁹ a limitation of this method is the triggering of immune responses against the radiotracer, which we considered undesirable.

By applying a similar gating strategy to that of Demberg *et al.*⁷ for the identification of nonhuman primate B cells in SLTs, we observed that the axillary and inguinal LNs of Doxo-treated macaques were comparable to those of saline-treated animals in terms of lymphocyte population sizes and IgG-secreting MBC numbers. Also, regardless of treatment, activated-to-resting MBC ratios were inverted in the two SLT types: the spleen contained higher ratios of activated MBC, while LNs contained higher resting MBC ratios. In contrast to the LNs, we found altered lymphocyte populations in the spleens of animals following Doxo exposure several months ago. The terminal half-life of Doxo in the spleen of rhesus macaques is not known. Pharmacokinetic modelling in rabbits, which was able to cross-predict human plasma levels of Doxo, showed a terminal Doxo half-life of between 20 and 48 h, with similar elimination half-lives in the animals' plasma, spleen, liver, lung, heart and lean tissues.²⁰ Tissue distribution of Doxo shortly after *i.v.* administration into healthy rats has shown that the spleen contains Doxo concentration 10 times higher than that in serum.¹⁸ In addition, a predominant loss of splenic marginal-zone B cells has been noted in normal rats after a single-dose Doxo infusion,²¹ and both transient and chronic Doxo exposure in healthy CD57BL/J6 mice triggered contraction of spleen mass, GC areas and marginal-zone macrophages.²² A study assessing the distribution of Doxo in different organs of *i.v.*-treated solid tumor patients reported high drug concentrations in LNs relative to muscle and bone marrow, while spleen sections were not examined.¹⁷ Thus, even if it is established that LNs and spleen have different capacities to filter blood, it is challenging to draw firm conclusions as to why LNs are less altered by, or recover faster from, Doxo treatment than the spleen. Nevertheless, at the multicellular level, an intact GC morphology and area were noted in Doxo-treated macaques, with noticeable clusters of proliferating B cells. This

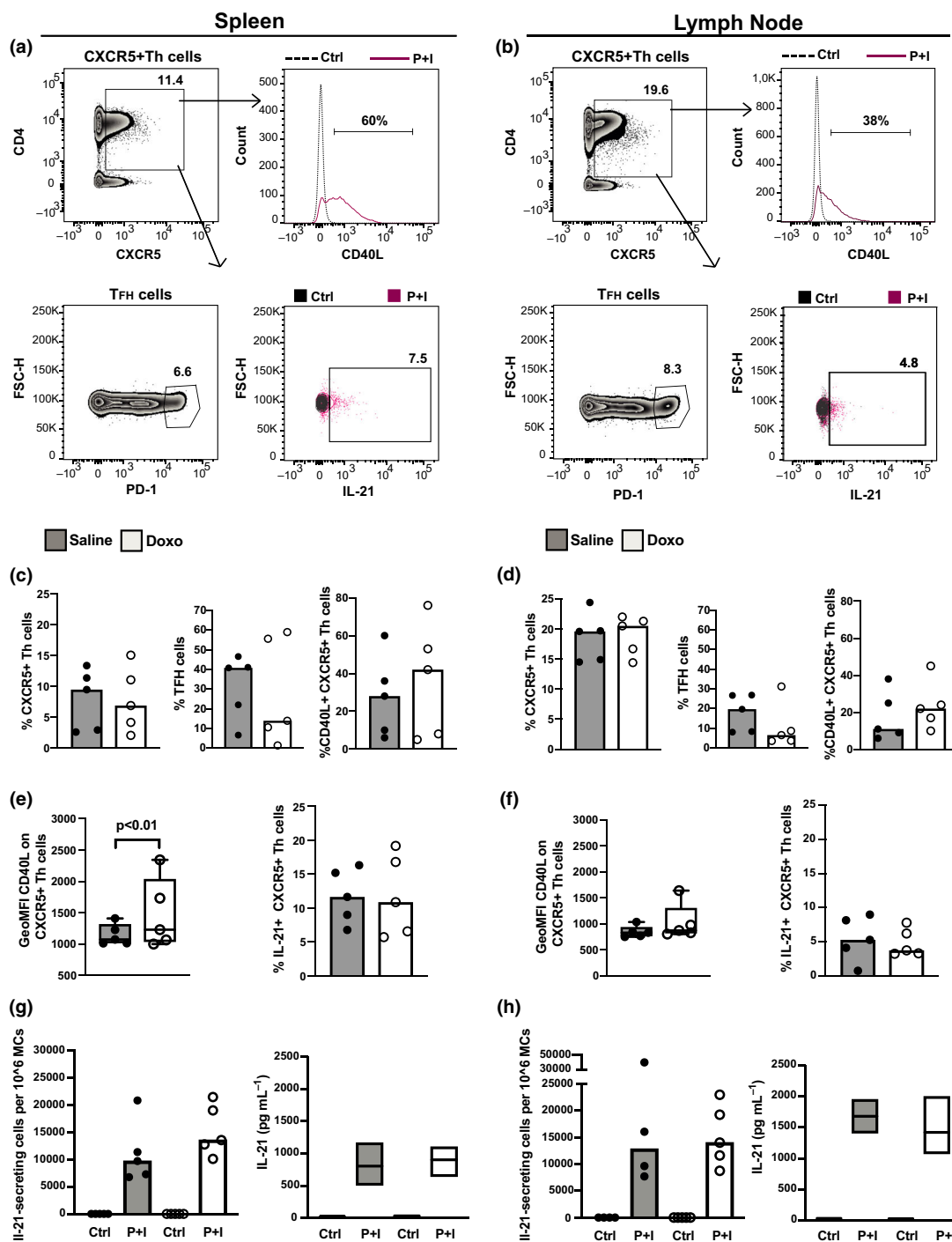


Figure 3. Immunophenotype and functional analysis of spleen and LN-derived CXCR5⁺ Th and T_{FH} cells from Doxo- and saline-treated macaques. Representative gating strategy for (a) spleen and (b) LN from rhesus macaques ($n = 10$) 5 months postchemotherapy completion ($n = 5$ Doxo- and 5 saline-treated, 2 technical replicates per condition). Compiled data from FACS analyses of spleen (c, e) and LN (d, f) CXCR5⁺ Th and T_{FH} cells from Doxo (open circles)- and saline (filled circles)-treated macaques. IL-21 production in spleen (g) and LN (h). IL-21-producing MC numbers (left-hand side in g, h) determined by ELISPOT ($n = 4$ or 5 animals per group, 2–4 replicates per condition), and IL-21 in MC cultures (right-hand side in g, h) quantified by ELISA ($n = 3$ animals per group, 2 replicates per condition). Ctrl, cell culture medium; P + I, PMA + ionomycin.

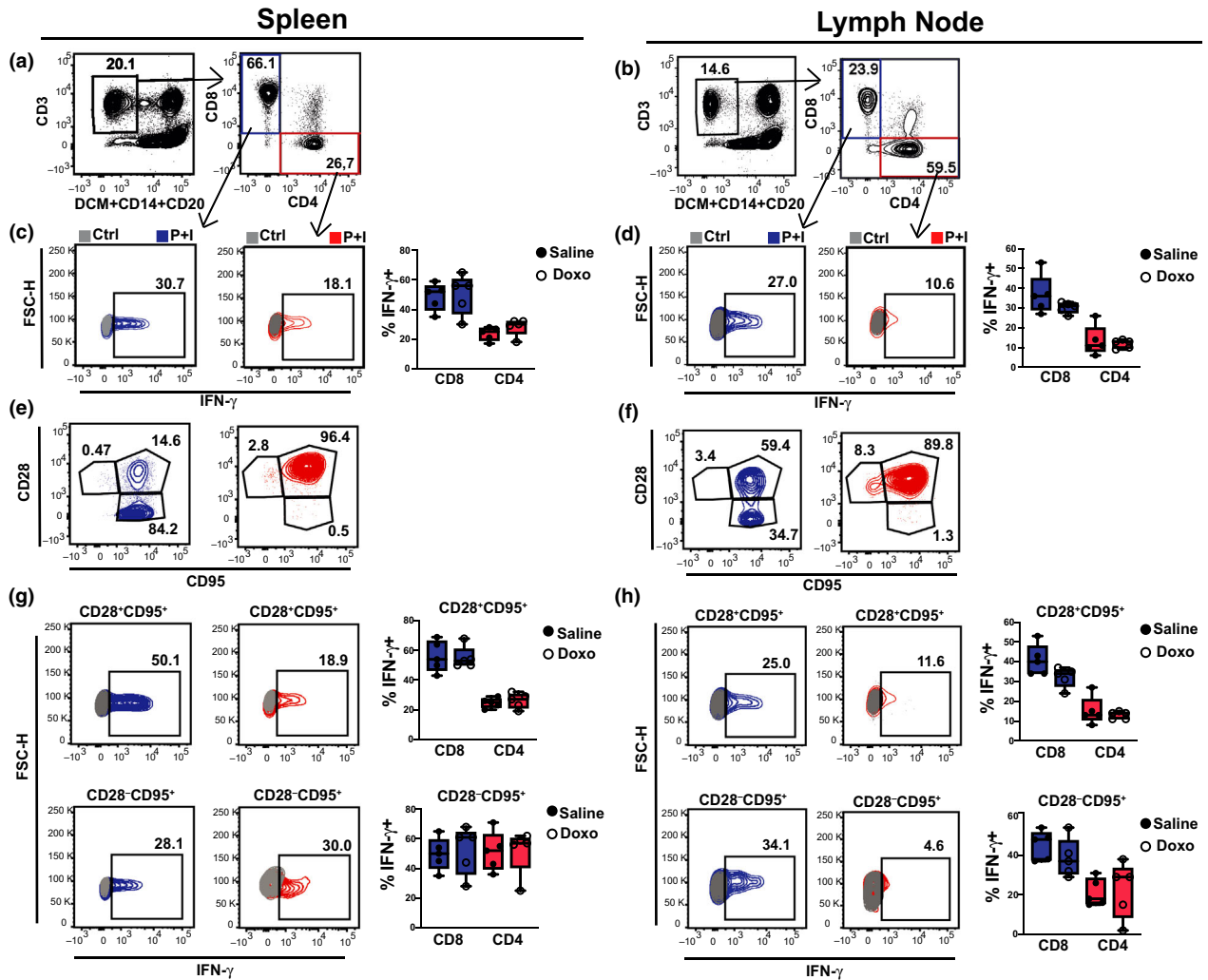


Figure 4. Immunophenotype and functional analysis of spleen and LN-derived T cells following cessation of anthracycline therapy. Cytotoxic (CD8⁺, blue) and helper (CD4⁺, red) T cells from Doxo (open circles)- and saline (filled circles)-treated macaques ($n = 5$ animals per group, 2 technical replicates for each condition). Representative FACS gating strategy for spleen (a, c, e, g) and LN (b, d, f, h) from the same animal 5 months postchemotherapy. Compiled data from FACS analyses of spleen (box plot in c) and LN (box plot in d) IFN- γ ⁺ CD8 and CD4 T cells in Doxo- and saline-treated macaques. Compiled data of spleen (box plots in g) and LN (box plots in h) IFN- γ ⁺ T-cell phenotypes containing enriched T_{CM} (CD28⁺CD95⁺) and T_{EM} (CD28⁻CD95⁺) cells in Doxo (open circles)- and saline (filled circles)-treated macaques. Ctrl, cell culture medium; P + I, PMA + ionomycin.

could be the result of a general rebound in cell numbers, as commonly seen in the blood after chemotherapy, or related to more specific changes in the GC microenvironment. The presence of intact GCs contrasts with the lower IgG-secreting MBC ratios found in the Doxo-exposed animals, and a defect in the transition of activated B cells to MBCs may be one possible explanation.

We found a lower proportion of splenic CD27⁺ and IgG⁺ B cells in macaques exposed to Doxo nearly six months earlier. These findings were in line with the lower numbers of total and measles-

specific MBCs, but not with their TT-specific counterparts or the overall size of ASCs. It remains an open question as to whether the ASCs are short-lived, originate from a pre-existing MBC pool or stem from GC reactions that have not involuted following re-immunisation of the animals. A preserved ability to form MBCs against *de novo* antigen (TT) one month after chemotherapy cessation may be explained by a GC response that is sustained long enough to allow B-cell recovery, MBC generation and differentiation to PCs. Thus, regardless of whether there were insufficiencies or

not in the recovery of marginal-zone cells like macrophages postchemotherapy, such as that seen in mice and rats,^{21,22} we anticipated that B-cell responses raised against T-cell-dependent vaccine antigens such as TT and measles would be intact in Doxo-treated macaques. The mechanisms underpinning a poorer antibody response from splenic MBCs to a recall antigen is unclear but could speculatively be because of a range of B-cell-intrinsic^{23,24} or B-cell-extrinsic factors^{25,26} additionally influenced by anthracycline therapy. For instance, it is conceivable that the precursors of anti-TT IgG-secreting cells consisted of newly generated MBCs, that is the ones not previously exposed to Doxo, whereas those against measles belonged to an MBC compartment formed years before. MBCs are, through decreased expression of checkpoint inhibitors, wired to enter cell division earlier than naïve B cells.²⁷ In agreement with findings on telomere dysfunction in normal lymphocytes following exposure to Doxo,²⁸ there is a possibility that anthracycline exposure may negatively impact the genetic stability of MBCs formed before chemotherapy. An altered trafficking of pre-existing MBCs upon Doxo exposure as a consequence of changed cell motility, reported in other cells of the immune system,²⁹ may be another possibility. Lastly, a study on secondary MBC responses to measles showed that MBCs from healthy adult donors proliferated after stimulation of the B-cell receptor together with T-cell cytokines, but failed to produce antibodies after coligation with CD40L.²⁵ We were limited by means of sample size to test whether a lower proportion of measles-specific MBCs could be a result of the marked CD40L upregulation by CXCR5⁺ Th cells seen in the spleens of Doxo-treated animals. Whether the decreased MBC frequency in Doxo-treated animals is because of an increase in other cell type populations not assessed here remains an open question. The bulk population of T cells in SLTs were largely unaffected by prior Doxo treatment, and the reason behind differential T- and B-cell sensitivity to Doxo, or possibly that between B cells across different SLTs, needs attention in future studies.

We acknowledge the limitations represented by the lack of additional components in the treatment regimen and follow-up time. Whether anthracyclines alone can represent the chemotherapy-caused alterations in adaptive memory function following ALL treatment remains an open question. However, anthracyclines serve as important components of

current international treatment protocols for ALL, both during the induction and intensification phases. This drug class induces profound bone marrow toxicity, which greatly impacts on myelopoiesis and lymphopoiesis; since anthracyclines lack selectivity for cancer cells, they could negatively impact the function of normal cells and tissues. Even though the contribution of spleen to B-cell antigen-recall responses was incompletely studied, it is arguable whether an altered splenic MBC population would have any clinical significance in vaccine responses in ALL survivors.^{30–32} Nonetheless, our study contributes to understanding the effect of anthracycline on various tissues that are central to the formation and maintenance of immunological memory, by the use of a large animal model like the macaque in a prospective and controlled setting. Based on our findings, we propose that, in contrast to the bone marrow, blood and LNs of the same examined animals,¹¹ the splenic lymphocyte populations are more severely altered by anthracycline treatment. Similar to findings from Donahue *et al.*,¹⁹ who focused on T-lymphocyte recovery postirradiation, we appreciate that the recovery of MBC populations differs between the blood and spleens of previously immunocompromised macaques in terms of diminished splenic IgG⁺ MBCs after only three doses of anthracycline infusion.

METHODS

Animals, treatment protocol and tissue sampling

Following ethical approval by the Institutional Animal Care and Use Committee at the Biomedical Primate Research Centre, the Netherlands (DEC#627 BPRC), 10 adult male macaques (*Macaca mulatta*, 11–15 years) were included in this prospective study. The animals were followed for a total of 211 days, during which BM toxicity and systemic side effects were evaluated and consecutive serum, blood and bone marrow samples were taken as previously described.¹¹ All macaques were measles-immune after vaccination during infancy, but tetanus and rubella were naïve at the time of inclusion. They were then divided into two groups based on matched weight and baseline anti-measles IgG titres. The first group ($n = 5$, from now on referred to as the Doxo group) received doxorubicin hydrochloride (Mylan, Stockholm) in a saline infusion lasting 60 min, for a total of 3 times, at 28- to 30-day intervals. Doxo dosage was increased during each cycle, starting with a dose of 30 mg m⁻² in the first cycle, 50 mg m⁻² in the second cycle and 75 mg m⁻² in the third cycle. The weight of all animals as well as their absolute white blood, CD20⁺ and CD27⁺ cell counts were registered continuously. Nadir

occurred 10–15 days after each Doxo infusion.¹¹ The second group ($n = 5$, from now on referred to as the saline group) received only saline under otherwise identical conditions as the Doxo group. Twenty-eight days after the last Doxo dose, all animals were vaccinated with 0.5 mL subcutaneous M.M.RVaxPro[®] (Sanofi Pasteur MSD SNC, Lyon) and 0.5 mL intramuscular tetanus toxoid (TT) vaccine (Netherlands Vaccine Institute, Bilthoven). At the end of the study (day 211), the animals were euthanised by pentobarbital overdose. Lymph nodes (LNs, axillary and/or inguinal LNs) and spleens were removed. Each spleen was cut in half for immunohistology or mononuclear cell (MC) isolation using the standard Ficoll-Paque method. Isolated MCs from spleens and LNs were suspended in 10% DMSO and 90% foetal calf serum (FCS, both from Thermo Fisher Scientific, Dreieich), aliquoted and cryopreserved in liquid nitrogen until downstream assays. Tissues were embedded in OCT compound (Tissue-Tek, Sakura, Alphen aan den Rijn) and stored at -80°C until processing for immunohistology.

Cell culture conditions

MCs from spleens and LNs were thawed, washed and resuspended in culture medium (RPMI 1640) supplemented with 10% FCS, L-glutamine (2 mmol L^{-1}), penicillin G sodium (100 U mL^{-1}) and streptomycin sulphate (100 g mL^{-1} , all from Thermo Fisher Scientific) to a concentration of 10^6 cells mL^{-1} . A proportion of MCs were activated with 10 ng mL^{-1} phorbol 12-myristate 13-acetate (PMA) and $1 \mu\text{g mL}^{-1}$ ionomycin (both from Merck, Stockholm) in the presence of protein transport inhibitor monensin (GolgiStop, BD Biosciences, Stockholm) for 4 h at 37°C and 5% CO_2 , ahead of flow cytometric analysis of T-cell subsets and their cytokines. MCs in culture medium with monensin or in culture medium alone served as nonstimulated controls or for immunophenotyping of B lymphocytes, respectively. To assess total and vaccine-specific IgG-secreting MBCs, MCs were pre-activated with $1 \mu\text{g mL}^{-1}$ resiquimod (R848) and 10 ng mL^{-1} IL-2 (both from Mabtech, Stockholm) in culture plates for 72 h. IL-2-secreting cells were enumerated after overnight activation of MCs with 10 ng mL^{-1} PMA and $1 \mu\text{g mL}^{-1}$ ionomycin directly into wells of pretreated and coated ELISPOT plates (details found below the ELISPOT heading). MCs in cell culture medium only served as negative controls in both cases. Following the activation steps and prior to ELISPOT, cell culture supernatants were collected and stored at -80°C .

Flow cytometry

Prior to labelling with pretitrated fluorescent antibodies, a dead cell marker (DCM, Thermo Fisher) was used to exclude nonviable cells from analysis. Details on Abs and clones used are to be found in Supplementary table 2. Mouse IgG1 isotype and FMO controls with alternating combinations of lineage markers in respective panels enabled appropriate gating of cell populations. All reagents were purchased from BD, Thermo Fisher, BioLegend (San Diego) and Santa Cruz Biotech (Heidelberg). Data were acquired through BD FACSVerser and analysed with FlowJo (BD Biosciences).

ELISPOT and ELISA

The proportions of IL-21-secreting cells and measles-specific, TT-specific and total IgG-secreting MBCs were determined using human IL-21 and IgG ELISPOT kits, respectively, following manufacturer's protocols (Mabtech). Briefly, IP filter plates (Merck) were activated and then coated overnight with IL-21 or IgG capture antibodies, or with $5 \mu\text{g}$ per well measles (Advanced Biotechnologies, Eldersburg MD) or $0.5 \mu\text{g}$ per well TT (code 04/150, NIBSC, Potters Bar) antigen. 50×10^3 MCs per well were added for detection of IL-21-producing cells, $20\text{--}25 \times 10^3$ pre-activated MCs per well were added for detection of IgG-producing cells, and $200\text{--}250 \times 10^3$ pre-activated MCs per well were added for detection of vaccine antigen-specific IgG-producing cells. All conditions were set up in 2–4 replicates. Nonstimulated MCs with otherwise matched conditions served as background controls. Following incubation overnight, visible spots were developed. Plates were analysed with CTL ImmunoSpot Micro Analyser (CTL, Bonn). Numbers of IgG-secreting MBCs were determined following subtraction of the total number of spots in IL-2 plus R848-stimulated wells with the number of spots in cell culture medium (Ctrl) wells which consisted of spontaneous antibody-secreting cells (ASCs). Data are presented as spots per 10^6 MCs. The percentage of antigen-specific IgG-secreting MBCs was determined by the division of TT or measles-specific IgG-secreting MBC over total IgG-secreting MBC numbers. Levels of antibodies and cytokines in supernatants were measured with NHP IgA, human IgG, IL-4, IL-21 and TGF- β ELISA kits according to the manufacturer's instructions (Mabtech). BAFF and CXCL12 in serum samples from the day of euthanasia were measured using ELISA kits according to the manufacturer's instructions (R&D systems, Abingdon).

Immunohistology

Ten- μm sections were cut and collected on noncoated glass slides (Thermo scientific, Menzel Gläser), then air-dried at RT for 2 h and subsequently fixed in cold 4% paraformaldehyde for 10 min. Slides were washed in cold PBS for 10 min at RT, rinsed once with cold PBS, then dried for 1.5 h and subsequently stored frozen until staining. For staining, slides were thawed and washed with perm/wash buffer consisting of Tris-buffered saline with 1% HEPES and 0.1% saponin (Merck). The same wash procedure followed each step unless otherwise stated. Tissues were blocked with 1% FCS. Endogenous biotin was blocked with Avidin/Biotin Blocking Kit (Vector Laboratories, Burlingame) according to the manufacturer's instructions. Incubation with primary antibodies occurred overnight at 4°C . Following blocking with 1% donkey serum and incubation with biotinylated secondary antibodies, streptavidin-conjugated fluorophores were added. This staining process was repeated for each marker (reagents listed in Supplementary table 2). After staining, slides were washed in distilled water, air-dried, then mounted using ProLong Diamond Antifade Medium with DAPI (Thermo Fisher Scientific) and stored in the dark at 4°C until imaging. Tiled images were acquired using a Nikon Eclipse Ti-E confocal microscope. GCs were analysed as previously described.^{33,34}

Briefly, multichannel confocal images were preprocessed using Fiji/ImageJ to render flattened three-colour overlays. Quantitative analysis was carried out using CellProfiler™ software (Broad Institute, Cambridge) with an algorithm developed in-house. In accordance with procedures previously established by us and others, GCs were defined as clusters of CD3⁺PD1⁺ cells and CD3⁻Ki67⁺ cells, which – together with the tissue contours – were defined manually.³³ Enumeration of cells was done by automated image analysis. Data output was further processed using in-house Java software.

Statistics

Following evaluation of data distribution, parametric one-way or nonparametric Kruskal–Wallis ANOVA was applied to test the statistical differences between multiple generated variables from the (Doxo) treated and control (saline) groups. Statistical differences were considered if *P*-values were < 0.05 after correction for multiple comparisons (Dunn's or Bonferroni). For the immunohistological analyses, Mann–Whitney *U*-test was applied. All lines and bars represent the median, except in the immunohistology data where they represent geometric mean values. Analyses were carried out using GraphPad Prism (v.8, San Diego). Agglomerative hierarchical cluster analysis and principal component analysis of spleen and LN B-cell populations were based on flow cytometry data. Cluster calculation was carried out using the average link function and Euclidean distance by *hclust* and visualised with *fviz_dend*. Principal components were assessed with *prcomp*. Both were analysed with R version 3.6.0.

CONCLUSION

The findings from this study imply that previous exposure to anthracycline, a widely used agent in the treatment of childhood ALL, negatively imprints the function of splenic MBCs.

ACKNOWLEDGMENTS

We thank Francesca Chiodi, Carina Bengtsson and Pontus Hedberg at Biomedicum, Karolinska Institutet, for technical assistance and arranging entry to the required laboratory facilities, and Jacqueline Wubben at BPRC, for assistance with immunohistology. This work was supported by PRIMOCID (EUPRIM-NET, number 026155, AN), the Swedish Research Council (grant 2017-02001, AN, and 2015-02608, KL), the Swedish Childhood Cancer Foundation (grant 2014-0112, AN), the Swedish Cancer Society (grant 2017/460, ESE), the Stockholm County through the ALF agreement (grant 2015-0239, AN) and Karolinska Institutet Foundations & Funds (AN).

CONFLICT OF INTEREST

The authors declare no conflict of interest.

AUTHOR CONTRIBUTIONS

Gintare Lasaviciute: Data curation; Formal analysis; Methodology; Writing-original draft. **Andreas Lillieroth Bricaud:** Formal analysis; Methodology; Writing-original draft. **Fredrika Hellgren:** Data curation; Formal analysis; Methodology; Writing-original draft. **Hanna Murén Ingelman-Sundberg:** Formal analysis; Methodology; Writing-original draft. **Staffan Eksborg:** Conceptualization; Supervision; Writing-original draft. **Margreet Jonker:** Data curation; Methodology; Project administration; Resources; Supervision; Writing-original draft. **Krista G. Haanstra:** Data curation; Methodology; Project administration; Resources; Supervision; Writing-original draft; Writing-review & editing. **Ida Hed Myrberg:** Formal analysis; Software; Writing-original draft. **Eva Sverremark-Ekström:** Funding acquisition; Investigation; Resources; Supervision; Writing-original draft; Writing-review & editing. **Karin Lore:** Funding acquisition; Investigation; Resources; Supervision; Writing-original draft; Writing-review & editing. **Shanie Hedengren:** Conceptualization; Data curation; Formal analysis; Funding acquisition; Investigation; Methodology; Project administration; Supervision; Visualization; Writing-original draft; Writing-review & editing. **Anna Nilsson:** Conceptualization; Data curation; Formal analysis; Funding acquisition; Investigation; Project administration; Resources; Supervision; Writing-original draft; Writing-review & editing.

REFERENCES

1. Saghafian-Hedengren S, Söderström I, Sverremark-Ekström E, Nilsson A. Insights into defective serological memory after acute lymphoblastic leukaemia treatment: the role of the plasma cell survival niche, memory B-cells and gut microbiota in vaccine responses. *Blood Rev* 2018; **32**: 71–80.
2. Weisel FJ, Zuccarino-Catania GV, Chikina M, Shlomchik MJ. A temporal switch in the germinal center determines differential output of memory B and plasma cells. *Immunity* 2016; **44**: 116–130.
3. Wirths S, Lanzavecchia A. ABCB1 transporter discriminates human resting naive B cells from cycling transitional and memory B cells. *Eur J Immunol* 2005; **35**: 3433–3441.
4. Fecteau JF, Côté G, Néron S. A new memory CD27⁻ IgG⁺ B cell population in peripheral blood expressing V H genes with low frequency of somatic mutation. *J Immunol* 2006; **177**: 3728–3736.
5. Sanz I, Wei C, Lee FE, Anolik J. Phenotypic and functional heterogeneity of human memory B cells. *Semin Immunol* 2008; **20**: 67–82.
6. Weiss GE, Crompton PD, Li S et al. Atypical memory B cells are greatly expanded in individuals living in a malaria-endemic area. *J Immunol* 2009; **183**: 2176–2182.
7. Demberg T, Brocca-Cofano E, Xiao P et al. Dynamics of memory b-cell populations in blood, lymph nodes, and bone marrow during antiretroviral therapy and envelope boosting in simian immunodeficiency virus SIVmac251-infected rhesus macaques. *J Virol* 2012; **86**: 12591–12604.

8. Mahnke YD, Brodie TM, Sallusto F, Roederer M, Lugli E. The who's who of T-cell differentiation: human memory T-cell subsets. *Eur J Immunol* 2013; **4**: 2797–2809.
9. Vaccari M, Franchini G. T cell subsets in the germinal center: lessons from the macaque model. *Front Immunol* 2018; **9**: 1–11.
10. Stock W, La M, Sanford B et al. What determines the outcomes for adolescents and young adults with acute lymphoblastic leukemia treated on cooperative group protocols? A comparison of Children's Cancer Group and Cancer and Leukemia Group B studies. *Blood* 2008; **112**: 1646–1654.
11. Ingelman-Sundberg HM, Saghafian-Hedengren S, Jahnmatz M, Eksborg S, Jonker M, Nilsson A. Selective loss of vaccine-specific memory B cells in a rhesus macaque model of chemotherapy: influence of doxorubicin on immunological memory. *Haematologica* 2015; **100**: e158–e161.
12. Westermann J, Pabst R. Distribution of lymphocyte subsets and natural killer cells in the human body. *Clin Invest* 1992; **70**: 539–544.
13. Nilsson A, De Milito A, Nordin M et al. Current chemotherapy protocols for childhood acute lymphoblastic leukemia induce loss of humoral immunity to viral vaccination antigens. *Pediatrics* 2002; **109**: 1–6.
14. Sun M, Ma Y, Xu Y et al. Dynamic profiles of neutralizing antibody responses elicited in rhesus monkeys immunized with a combined tetravalent DTaP-Sabin IPV candidate vaccine. *Vaccine* 2014; **32**: 1100–1106.
15. de Swart RL. Measles: what we have learned from non-human primate models. *Drug Discov Today Dis Model* 2017; **23**: 31–34.
16. Donelli MG, Martini A, Colombo T, Bossi A, Garattini S. Heart levels of adriamycin in normal and tumor-bearing mice. *Eur J cancer* 1976; **12**: 913–923.
17. Lee YN, Chan KK, Harris PA, Cohen JL. Distribution of adriamycin in cancer patients. *Cancer* 1980; **45**: 2231–2239.
18. Sonneveld P, Van Bekkum DW. Different distribution of adriamycin in normal and leukaemic rats. *Br J Cancer* 1981; **43**: 464–470.
19. Donahue RE, Srinivasula S, Uchida N et al. Discordance in lymphoid tissue recovery following stem cell transplantation in rhesus macaques: an *in vivo* imaging study. *Blood* 2015; **126**: 2632–2641.
20. Harris PA, Gross JF. Preliminary pharmacokinetic model for adriamycin (NSC-123127). *Cancer Chemother Rep* 1975; **59**: 819–825.
21. Dammers PM, De Boer NK, Deenen GJ, Nieuwenhuis P, Kroese FGM. The origin of marginal zone B cells in the rat. *Eur J Immunol* 1999; **29**: 1522–1531.
22. Jadapalli JK, Wright GW, Kain V et al. Doxorubicin triggers splenic contraction and irreversible dysregulation of COX and LOX that alters the inflammation-resolution program in the myocardium. *Am J Physiol Circ Physiol* 2018; **315**: H1091–H1100.
23. Roy MP, Kim CH, Butcher EC. Cytokine control of memory B cell homing machinery. *J Immunol* 2002; **169**: 1676–1682.
24. Good-Jacobson KL. Strength in diversity: phenotypic, functional, and molecular heterogeneity within the memory B cell repertoire. *Immunol Rev* 2018; **284**: 67–78.
25. Silvy A, Lagresle C, Bella C, Defrance T. The differentiation of human memory B cells into specific antibody-secreting cells is CD40 independent. *Eur J Immunol* 1996; **26**: 517–524.
26. Auladell M, Nguyen TH, Garcillán B, Mackay F, Kedzierska K, Fox A. Distinguishing naive- from memory-derived human B cells during acute responses. *Clin Transl Immunol* 2019; **8**: e01090.
27. Good-Jacobson KL, Chen Y, Voss AK, Smyth GK, Thomas T, Tarlinton D. Regulation of germinal center responses and B-cell memory by the chromatin modifier MOZ. *Proc Natl Acad Sci USA* 2014; **111**: 9585–9590.
28. Li P, Hou M, Lou F, Björkholm M, Xu D. Telomere dysfunction induced by chemotherapeutic agents and radiation in normal human cells. *Int J Biochem Cell Biol* 2012; **44**: 1531–1540.
29. Mendonça MAO, Souto FO, Micheli DC et al. Mechanisms affecting neutrophil migration capacity in breast cancer patients before and after chemotherapy. *Cancer Chemother Pharmacol* 2014; **73**: 317–324.
30. Wasserstrom H, Busse J, Lim LC-L, Cunningham-Rundles C. Memory B cells and pneumococcal antibody after splenectomy. *J Immunol* 2008; **181**: 3684–3689.
31. Giesecke C, Frölich D, Reiter K et al. Tissue distribution and dependence of responsiveness of human antigen-specific memory B cells. *J Immunol* 2014; **192**: 3091–3100.
32. Madenci AL, Armstrong LB, Kwon NK et al. Incidence and risk factors for sepsis after childhood splenectomy. *J Pediatr Surg* 2019; **54**: 1445–1448.
33. Lindgren G, Ols S, Liang F et al. Induction of robust B cell responses after influenza mRNA vaccination is accompanied by circulating hemagglutinin-specific ICOS⁺ PD-1⁺ CXCR3⁺ T follicular helper cells. *Front Immunol* 2017; **8**: 1539.
34. Lindgren G, Ols S, Thompson EA, Loré K. Comparative analysis of the germinal center response by flow cytometry and immunohistology. *J Immunol Methods* 2019; **472**: 16–24.

Supporting Information

Additional supporting information may be found online in the Supporting Information section at the end of the article.



This is an open access article under the terms of the Creative Commons Attribution-NonCommercial-NoDeriv License, which permits use and distribution in any medium, provided the original work is properly cited, the use is non-commercial and no modifications or adaptations are made.